CHEMISTRY OF MATERIALS

pubs.acs.org/cm

Article

Deposition of N-Heterocyclic Carbenes on Reactive Metal Substrates—Applications in Area-Selective Atomic Layer Deposition

Justin T. Lomax, Eden Goodwin, Mark D. Aloisio, Alex J. Veinot, Ishwar Singh, Wai-Tung Shiu, Maram Bakiro, Jordan Bentley, Joseph F. DeJesus, Peter G. Gordon, Lijia Liu, Seán T. Barry,* Cathleen M. Crudden,* and Paul J. Ragogna*

Cite This: *Chem. Mater.* 2024, 36, 5500−5507

Read Online

ACCESS | Metrics & More | Article Recommendations | Supporting Information

ABSTRACT: Integrated circuits are presently constructed using top-down strategies composed of multiple etching and lithographic steps. As the feature sizes of these devices approach single-digit nm scales, existing fabrication methods introduce defects which require further corrective steps and are rapidly becoming ineffective for industry needs. To meet future scaling requirements, bottom-up fabrication methods which leverage differences in the local surface environment such as area-selective atomic layer deposition (AS-ALD) are promising but have been limited by the surface-binding energies of adsorbates. N-heterocyclic carbenes (NHCs) have shown excellent bonding to metal surfaces and are presented herein as next-generation carbon-based small molecule inhibitors (SMIs) for use in AS-ALD processes. NHCs demonstrate a preference for adsorbing onto metal surfaces over dielectric materials and enable the selective deposition of ZnO onto SiO_2 bands. NHC-based SMIs can be effectively removed by either thermal annealing at 350 °C or plasma treatment using hydrogen at 800 W for 60 s.

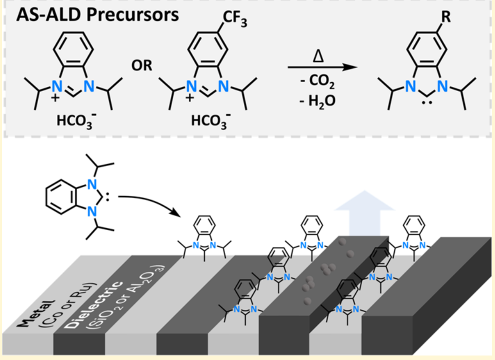

■ INTRODUCTION

Metallic surfaces, nanoparticles, nanoclusters, and single-atom molecular metal complexes are typically functionalized by organic ligands to stabilize and protect the reactive metal surfaces.[1−4] In the world of small molecules, ligands such as phosphines and N-heterocyclic carbenes (NHCs) are frequently used,[5−8] while metal surfaces and nanomaterials are typically protected with thiol-based ligands.[1,9,10] Recent studies from our group and others have demonstrated that NHCs are unique in their ability to react with and protect metals at all size regimes.[11−26]

Most of the work reported to date describing NHC overlayers on planar surfaces has focused on coinage metals, with platinum being the only reactive metal explored outside of this group.[13,14,16,27] This is despite the fact that molecular chemistry and nanoparticle work suggest that NHCs should form strong bonds to reactive metals such as Ru, Co, and other d-block metals (Figure 1A).[28−32] These surfaces have considerable importance in catalysis, but they are also poised to play a significant role in the construction of next-generation integrated circuits (ICs) for the semiconductor industry.[33−36] Both Co and Ru exhibit superior electrical and thermal conductivities when compared to Cu and are being explored to replace copper as an interconnect metal in the nanoregime. The reduced resistance and enhanced heat dissipation properties of Ru and Co contribute to improved device performance and energy efficiency.[36−39] Co and Ru are less susceptible to electromigration and diffusion, mitigating reliability issues that have always plagued Cu-based interconnects.[36,40−42] They are also superior to copper since they are not subject to decreases in conductivity at low dimensions.[43]

Modern integrated circuits (ICs) are built using complex three-dimensional nanostructures of interwoven metal and dielectric components, which require multiple repetitive steps of deposition, top-down patterning via masking and photolithography, and etching.[34,44,45] Devices featuring 3 nm processes are being put into production this year.[46] At these nanometer length scales, existing fabrication methods and materials are problematic. Specifically, issues related to top-down lithographic mask misalignment (e.g., edge placement errors, EPE, Figure 1B) pose a serious threat to the production of these devices.[34,44,47]

Atomic layer deposition (ALD) is a powerful bottom-up deposition technique that enables thin film growth with excellent conformality and atomic-level control over film thickness.[48] Area-selective ALD (AS-ALD) in particular

Received: February 16, 2024
Revised: May 3, 2024
Accepted: May 7, 2024
Published: May 28, 2024

https://doi.org/10.1021/acs.chemmater.4c00412

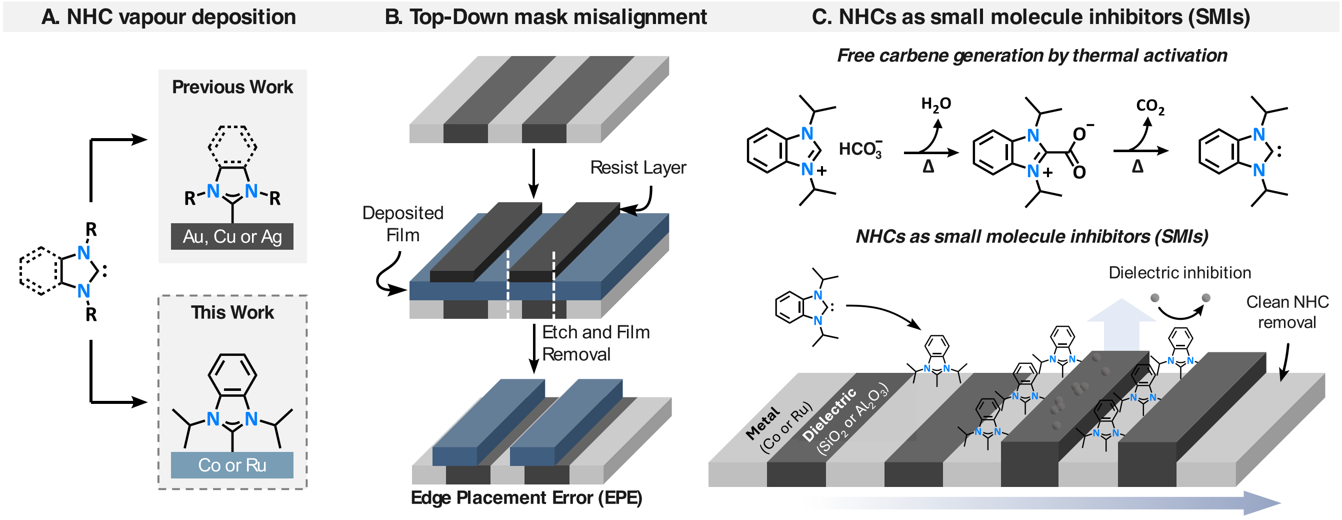

Figure 1. (A) Vapor deposition of NHCs onto metal surfaces. (B) Current top-down lithographic techniques that result in edge placement errors (EPEs). (C) Thermal activation of bicarbonate imidazolium salts to generate the free carbene with vapor deposition of NHCs as small molecule inhibitors (SMIs) on patterned metal/dielectric surfaces. Subsequent dielectric deposition is inhibited by the NHC monolayers enabling precise deposition of dielectric material.

(Figure 1B) has been explored to supplement lithography and reduce the use of chemical mechanical planarization.[44,49] AS-ALD leverages the differences in local surface energies by deactivating specific areas using small molecule inhibitors (SMIs), while other areas are built up.[44,49−53] This type of molecular mask has the potential to provide lateral precision at the scale of a single molecule.

The most widely examined SMIs for the protection of metal surfaces are thiol-based, providing selective functionalization and protection of metal surfaces.[51,52,54] However, thiols are prone to decomposition in oxidative environments, which leads to a loss of protective function and undesired growth on deactivated areas.[55,56] They can also form metal sulfides upon decomposition,[57,58] resulting in electron-rich sulfur impurities that cause high-resistance impurities in interconnects that diminish performance.[51] Due to the current issues with thiols, an urgent need arises to develop alternative SMIs for the protection of metal surfaces during device manufacturing.

Herein, we report our investigation into the use of NHCs to protect reactive metals, including those relevant to IC manufacturing. We show that NHCs are easily delivered in the gas phase and selectively functionalize Au, Co, and Ru surfaces in the presence of SiO_2 and Al_2O_3 dielectrics. NHC overlayers providing protection to the metallic regions during ZnO deposition and growth on dielectrics are demonstrated. The use of thermal annealing to improve selectivity at lower temperatures (175 °C) and cleanly remove the SMI at elevated temperatures or with plasma (>350 °C or 800 W, 60 s) is also presented. This collection of results underscores the potential of NHCs as SMIs for the next generation of AS-ALD processes.

■ RESULTS AND DISCUSSION

Self-assembled monolayers (SAMs) of NHCs prepared by deposition under ultrahigh vacuum conditions have been studied by several groups resulting in densely packed films with excellent thermal and chemical stability.[13,14,17,21,59,60] Small changes to the N-substituents and backbones can result in large changes in order and surface packing density, with codeposition experiments revealing the importance of intermolecular (likely CH−π) interactions to the formation of well-ordered SAMs.[13,14,17,25,59,61]

These characteristics suggested that NHCs would be good candidates for ALD processes; however, a detailed analysis of their thermal characteristics is lacking in the literature and deposition under more moderate vacuum conditions has not been described. Understanding their behavior on noncoinage metals is also critical. We began with an examination of bicarbonate benzimidazolium salts, as they are shelf-stable salts that can cleanly generate the free carbene in the gas phase via the liberation of H_2O and CO_2 (Figure 1C). This work focused on NHC precursors $^{\mathrm{iPr}}\mathrm{NHC}^{\mathrm{CF3}}\cdot\mathrm{HCO_3}$, which has a backbone CF_3 functional group, a substituent that has proven valuable as a spectroscopic handle appended to $^{\mathrm{iPr}}\mathrm{NHC}\cdot\mathrm{HCO_3}$.[27,59,61−63]

The thermal properties of these NHC precursors were examined by thermal gravimetric analysis (TGA) and differential scanning calorimetry (DSC; Figures 2 and S1). TGA is a particularly useful method to measure thermal events like

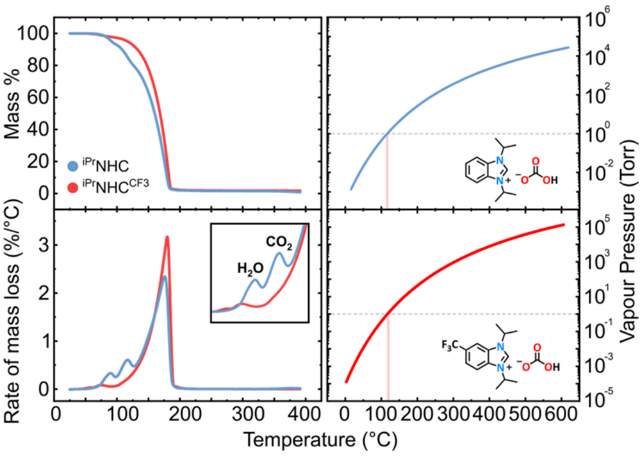

Figure 2. TGA traces of $^{\mathrm{iPr}}\mathrm{NHC}^{\mathrm{CF3}}\cdot\mathrm{HCO_3}$ and $^{\mathrm{iPr}}\mathrm{NHC}\cdot\mathrm{HCO_3}$ (left). One Torr vapor pressure plots of $^{\mathrm{iPr}}\mathrm{NHC}^{\mathrm{CF3}}\cdot\mathrm{HCO_3}$ and $^{\mathrm{iPr}}\mathrm{NHC}\cdot\mathrm{HCO_3}$ (right).

https://doi.org/10.1021/acs.chemmater.4c00412
Chem. Mater. 2024, 36, 5500−5507

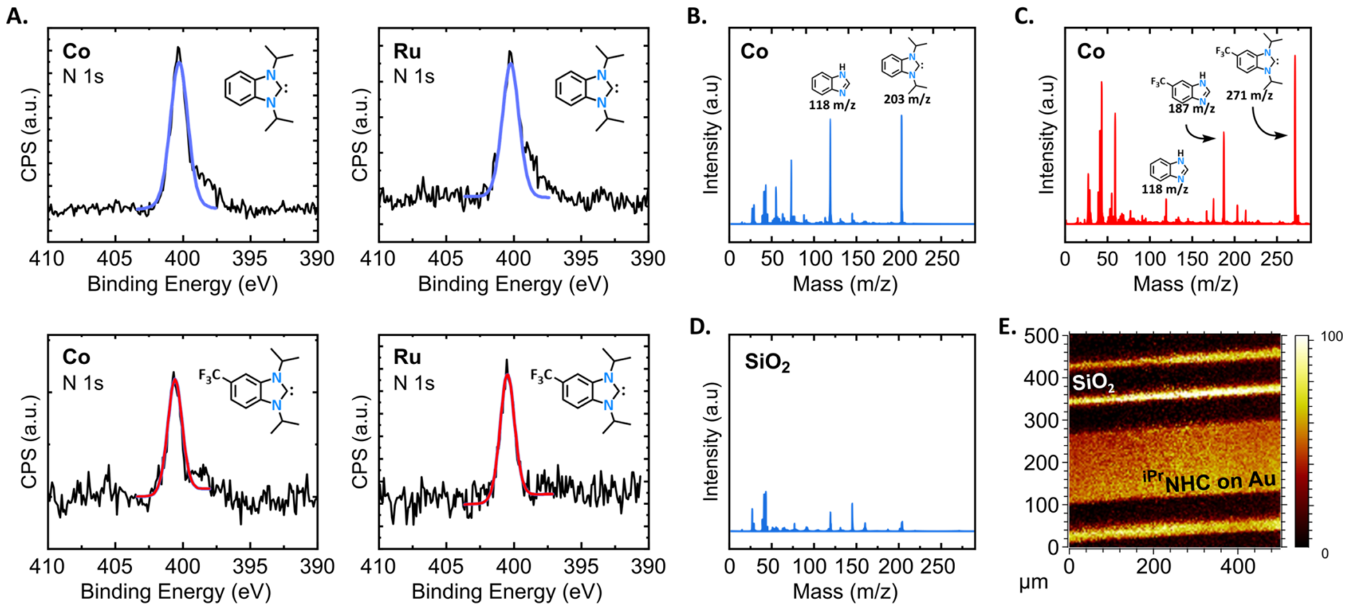

Figure 3. (A) Summary of XPS analysis completed for optimized ALD of $^{\mathrm{iPr}}$NHC$^{\mathrm{CF3}}$ and $^{\mathrm{iPr}}$NHC on Co and Ru substrates. The secondary ion mass spectrum of (B) $^{\mathrm{iPr}}$NHC deposition on a Co substrate with ions signals for M^+, loss of wingtip groups (C) $^{\mathrm{iPr}}$NHC$^{\mathrm{CF3}}$ deposition on a Co substrate with ions signals for M^+, loss of wingtip groups and (D) $^{\mathrm{iPr}}$NHC deposition on a SiO_x substrate with minimal M^+ ion signal. (E) ToF-SIMS image of selective deposition of $^{\mathrm{iPr}}$NHC on Au regions onto a variable patterned Au/SiO_2 substrate.

vaporization and decomposition under conditions that are relevant to vapor deposition. Samples are weighed while subjected to a programmable thermal profile (typically a thermal ramp). In the case of $^{\mathrm{iPr}}$NHC$^{\mathrm{CF3}}$·HCO_3, heating at a ramp rate of 10 °C/min to 400 °C provides a thermogram showing several thermal events attributed to the liberation of H_2O and CO_2 at 78 and 115 °C, followed by the onset of volatilization of the free carbene $^{\mathrm{iPr}}$NHC$^{\mathrm{CF3}}$ at 125 °C. The TGA trace for $^{\mathrm{iPr}}$NHC·HCO_3 showed the mass loss events of H_2O and CO_2 at 91 and 117 °C, respectively, followed by the volatilization of the free carbene ($^{\mathrm{iPr}}$NHC). $^{\mathrm{iPr}}$NHC$^{\mathrm{CF3}}$ and $^{\mathrm{iPr}}$NHC feature wide thermal windows (i.e., the temperature range between the onset of volatility and the onset of thermal decomposition) of 135 and 125 °C, respectively, and therefore are well-suited for vapor-phase depositions, as in ALD applications. To quantify the volatility, a model employing the rate of mass loss curve is used to derive vapor pressure plots.[64,65] Fitting the data against the Langmuir equation enables the determination of the temperature at which the precursor has a vapor pressure of 1 Torr (T_V; Figure 2). The determination of the 1 Torr vapor pressure for $^{\mathrm{iPr}}$NHC$^{\mathrm{CF3}}$ and $^{\mathrm{iPr}}$NHC is 110.6 and 109.2 °C, respectively, owing to the lower pressure conditions and the removal of CO_2 upon the formation of the carboxylate intermediate as part of the carboxylate and free carbene equilibrium.[63]

Vapor deposition behavior of NHCs was studied through a series of quartz crystal microbalance (QCM) saturation experiments on gold as a model substrate (Figures S20 and S21). The pulsed exposure of each NHC studied resulted initially in linear growth regimes until saturation, yielding areal densities of 3.4 and 3.2 NHC/nm^2 for $^{\mathrm{iPr}}$NHC$^{\mathrm{CF3}}$ and $^{\mathrm{iPr}}$NHC, respectively. These values closely align with previously recorded densities of NHC surfactants on similar amorphous surfaces (3.92 ± 0.12 NHC/nm^2).[12,62] Continued exposure led to an increase in these areal densities, suggesting the formation of multiple layers following the saturated monolayer is possible under these conditions. After saturation of the monolayer, the rate of deposition significantly decreases and implies that the shift in kinetics of the deposition of bi- and multilayer formation is much less favorable. From these observations, we have optimized the deposition conditions to 100 cycles of a 0.1 s pulse time of the corresponding NHC, followed by a 10 s purge to primarily maintain the window of monolayer formation.

We then explored the deposition of NHCs on Co and Ru films because they have been identified for their potential use in next-generation devices. Au substrates were employed as a reference metal since much of the NHC-on-metal work has employed gold.[15,18,27] Vapor deposition conditions were optimized in a commercial ALD tool, and the resulting films were characterized using X-ray photoelectron spectroscopy (XPS) and time-of-flight secondary ion mass spectrometry (ToF-SIMS).

Deposition of $^{\mathrm{iPr}}$NHC$^{\mathrm{CF3}}$on Au surfaces results in an N(1s) signal as a single peak at 400.4 eV, consistent with prior reports of the deposition of related NHCs (Figure S13).[13,19,66,67] The presence of the CF_3 substituent was confirmed by the observation of a monomodal signal at 688.1 eV F(1s) (Supporting Information, SI). Deposition of $^{\mathrm{iPr}}$NHC was carried out under the same conditions, with XPS confirming the presence of the NHC on support through a signal at 400.1 eV.

The higher stability of oxides on the surfaces of Co and Ru by comparison to Au meant that a robust in-tool surface cleaning procedure had to be developed (SI). On these Ru and Co surfaces, we deposited $^{\mathrm{iPr}}$NHC$^{\mathrm{CF3}}$ and $^{\mathrm{iPr}}$NHC using optimized conditions. The resulting samples were analyzed by XPS, giving N(1s) signals in the expected area ($^{\mathrm{iPr}}$NHC$^{\mathrm{CF3}}$ Co, Ru; 400.5, 400.4 eV and $^{\mathrm{iPr}}$NHC on Co, Ru; 400.3, 400.2 eV) (Figure 3A). An additional peak at 397.8 eV on Co surfaces is attributed to an adventitious nitrogen species present in the underlying film. Similar results were obtained for the deposition of the unfunctionalized $^{\mathrm{iPr}}$NHC, indicating that the surface chemistry and binding characteristics of these NHC

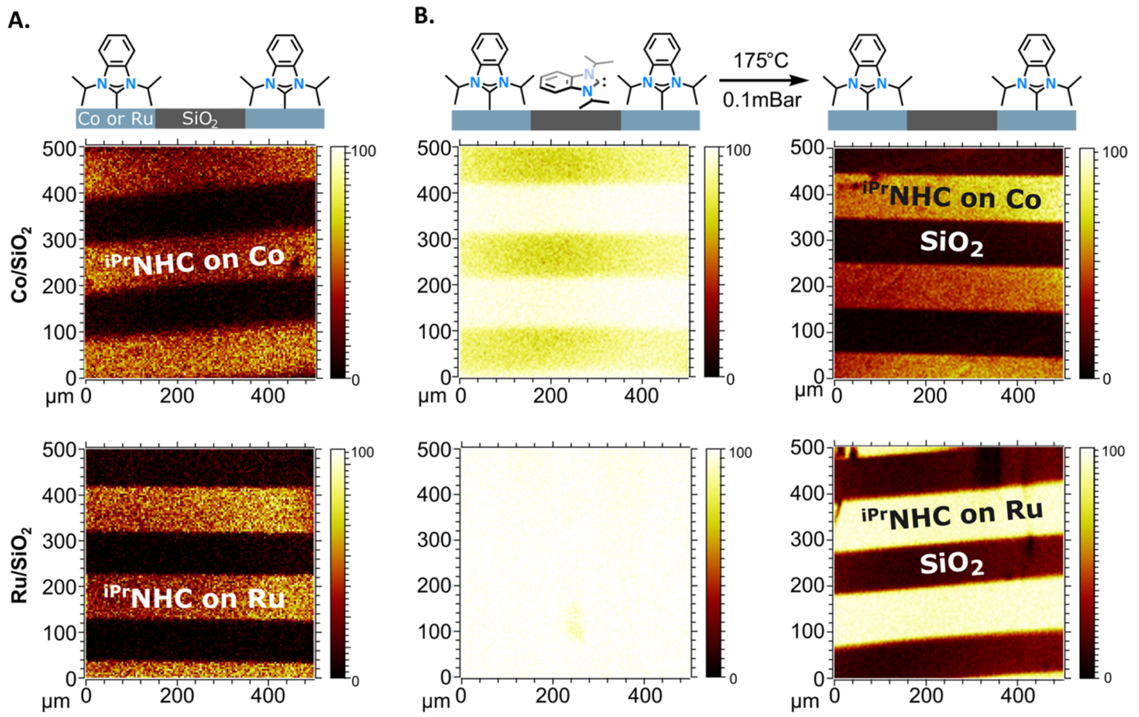

Figure 4. ToF-SIMS images of (A) selective deposition of ^{iPr}NHC on 100 μm metallic bands alternating with SiO_2 and (B) oversaturated deposition of ^{iPr}NHC onto patterned substrates before (left) and after (right) vacuum annealing at 175 °C under 0.1 mbar.

derivatives on Co and Ru surfaces are consistent across different functional groups, as shown in Figure 3B.

ToF-SIMS has the potential to provide the precise molecular formula of any surface species and is an ideal analytical technique for the evaluation of monolayers/thin films. Representative ToF-SIMS data for NHC depositions on a Co substrate are shown in Figure 3. Molecular ions that correspond to ^{iPr}NHC ($[M + H]^+ = 203$ m/z) were clearly observed on the metal surface (Figure 3B), and traces of the urea derived from the oxidation of ^{iPr}NHC were also detected on some samples (218 m/z) (Figure S6). This species was also observed when copper oxides were reduced with ^{iPr}NHC and likely were produced by the reaction of the NHC with residual surface oxides.[68] The molecular ion of ^{iPr}NHC^{CF3} was observed ($[M + H]^+ = 271$ m/z) along with the benzimidazole core (187 m/z) and CF_3 fragments (118 m/z; Figure 3C).

Having demonstrated that NHCs can be deposited on reactive metal surfaces, we aimed to establish the selectivity of their deposition in the presence of insulating/dielectric surfaces. Selective deposition is critical in the application of NHCs as small molecule inhibitors since they must protect the metal surface while leaving the dielectric uncovered, enabling growth on the latter in a subsequent deposition process. As an initial selectivity probe, we examined the deposition of ^{iPr}NHC on SiO_x and Al_2O_3. Under optimized conditions for deposition on Ru and Co, minimal chemisorption of ^{iPr}NHC was detected on these surfaces (Figure 3D). However, at higher dose numbers (100 cycles), surfaces begin to develop additional signals on dielectric and metal surfaces consistent with NHC hydrolysis and oxidation products (Figure S6). To gain insight into the selective placement of NHCs by ALD on patterned metal/dielectric interfaces, we prepared striped Au/SiO_2 surfaces. ToF-SIMS imaging was employed to map ^{iPr}NHC ($[M + H]^+ = 203$ m/z) on Au/SiO_2 following NHC deposition. High selectivity for deposition on Au in these patterned systems was observed (Figure 3E). ToF-SIMS analysis enabled the calculation of the selectivity coefficient as 0.97, where 1.00 would be the perfect selectivity for the metal (see SI for details).

Co and Ru patterned substrates with alternating patterns of metal (Co, Ru; 100 μm wide) and silicon (100 μm wide), in which the silicon surface is coated with native oxide (SiOx), were then utilized, as well as similarly patterned metal/Al_2O_3 substrates (Figures S11 and S12). After deposition with ^{iPr}NHC, the surfaces were again probed by ToF-SIMS. Molecular ions that corresponded to ^{iPr}NHC ($[M + H]^+ =$ 203 m/z) were localized on the metallic regions (Figure 4A). Low-intensity signals at 203 m/z were detected on the dielectric regions, which may suggest the presence of physiosorbed NHCs that resulted from the high NHC flux delivered to the surface. However, annealing to 175 °C for 1 h was highly effective at removing physisorbed NHC species selectively from the dielectric, resulting in a clean, well-defined monolayer on the metal portions of the patterned wafer (Figure 4B). ToF-SIMS mapping images illustrate the significant improvement in selectivity following an anneal, underscored by the obtained selectivity values of 0.85 for Co and 0.96 for Ru, which were determined by the relative ion intensity measurements between dielectric and metal regions. Even samples that were prepared specifically with a large excess of physisorbed NHCs can be cleaned up by a simple postdeposition vacuum annealing treatment (175 °C, 0.01 mbar, 30 min) (Figure 4B). Considering the observed increase in ion signal intensity, we hypothesize that this is indicative of a fully saturated NHC SMI layer, potentially accompanied by residual physisorbed NHCs. This interpretation is supported by the observed ion intensity and contrast, suggesting effective saturation of the metal surfaces.

We then investigated the ability of an Au/SiO_2 patterned substrate in which the metal is protected by ^{iPr}NHC-functionalization to resist dielectric nucleation on the metal bands (Figure 5). The substrate was subjected to 35 cycles of diethyl zinc (DEZ) and H_2O, resulting in a film growth of 6.5 nm with an approximate growth per cycle (GPC) of 1.9 Å. A patterned Au/SiO_2 film without any NHC protection shows the growth of ZnO over the entire surface on both the metal and dielectric (Figure 5). When analyzing the selectivity factor calculated for the growth of ZnO on SiO_x, it was determined to be $S = 0.89$ in NHC-protected systems, indicating a significantly enhanced resistance to undesired deposition. This contrasts with the $S = -0.10$ observed for ZnO growth on unprotected Au/SiO_2, where the negative value signifies a preference for the Au bands over the SiO_x.

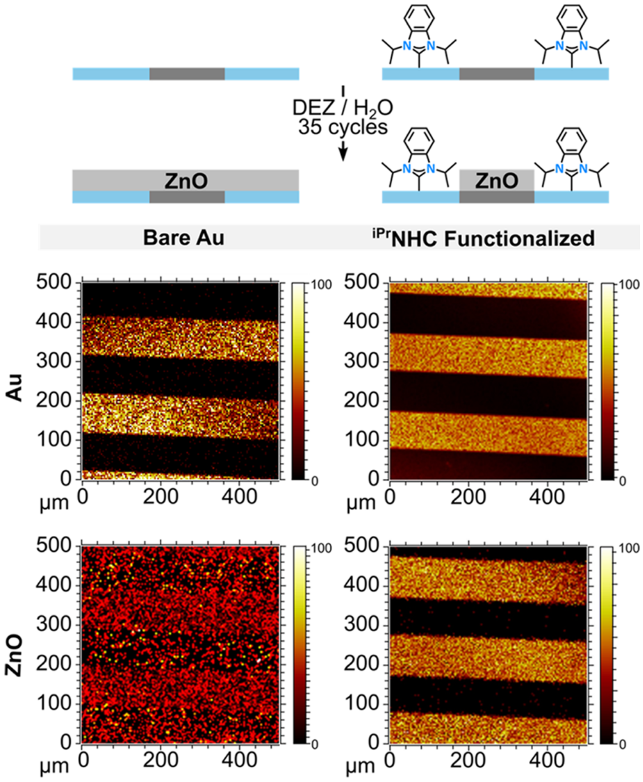

Figure 5. Diethyl zinc/H_2O deposition onto ^{iPr}NHC Au/SiO_2 with ToF-SIMS images of postdeposition of 35 cycles of ZnO onto bare and ^{iPr}NHC functionalized patterned Au/SiO_x.

To be effective for the temporary protection of metal surfaces, it is essential to remove the SMI prior to further processing. Surfaces annealed to 350 °C for 1 h or briefly exposed to a H_2/Ar plasma (800 W, 60 s) show that the ^{iPr}NHC monolayer can be cleanly removed, as indicated by the absence of the M^+ ion in ToF-SIMS and the absence of the N signal, as shown in the N 1s XPS spectra (Figures S16 and S18).

In conclusion, we have described the first examples demonstrating NHCs as effective SMIs on planar Co and Ru surfaces, which are critically important metals in the design of the next generation of interconnect materials for ICs. Selective vapor deposition of NHCs on Co and Ru surfaces in the presence of SiO_2 and Al_2O_3 dielectrics was achieved, with selectivity confirmed using XPS and ToF-SIMS. Postdeposition annealing assisted in removing physiosorbed NHC on dielectric surfaces, resulting in selectivity factors of 0.85 and 0.96 for Co and Ru, respectively. The presence of the NHC on metal surfaces was effective as an inhibitor against dielectric film growth (ZnO), and the NHC could be removed either thermally or after plasma treatment. These results lay the groundwork for the continued development of NHCs in AS-ALD applications and offer an excellent opportunity for the fabrication of robust micropatterns using bottom-up masking for area selective deposition and microelectronic pattern transfer.

■ MATERIALS AND METHODS

General Deposition of NHCs by ALD. All depositions were performed on a Picosun R-200 Advanced Plasma-Enhanced Atomic Layer Deposition (PE-ALD) tool. All wafers were exposed to a H_2/Ar plasma treatment (850W, 60 cycles) prior to deposition to reduce the surface oxides and remove any unwanted surface contaminants.[4] The deposition process starts with a nitrogen flush step, repeated three times, where the chamber is filled with nitrogen to a pressure of 100 hPa and then reduced to base pressure. The bubbler and chamber are then heated to their set points, heated to 90 and 150 °C, respectively, for 20 min before deposition. The deposition process consisted of a plasma clean, followed by short pulses of the NHC, and separated by 1 s purge steps. Precursor pulse, purge, and line flows used 99.998% N_2 (150 sccm). The NHC precursor pulse and purge times were 0.1 and 10 s, respectively, from a "PicoSolid" bubbler. Ten pulse/purge pairs were used. The plasma used a 6.0 argon carrier gas and a 5% hydrogen in argon mixture supplied by Praxair. The plasma was pulse/purged 100 times, using 14 s pulses at 800 W and 2 s purges. Each 14 s pulse consisted of two steps: a 1.4 s "stabilization time" and 12 s "RF power on" step.

X-ray Photoelectron Spectroscopy (XPS). The XP spectra were acquired at Surface Science Western (SSW) with a Kratos AXIS Supra X-ray photoelectron spectrometer using a monochromatic aluminum Kα source (15 mA, 15 kV). Sample analysis is measured from a depth of 7−10 nm with detection limits ranging from 0.1 to 0.5 atomic percent. The instrument work function was calibrated to give a binding energy (BE) of 284.8 eV for C (1s) C−C/C−H peaks. The Kratos charge neutralizer system was used on all specimens. Both the survey scan and high-resolution analyses were collected at a takeoff angle of 90° with an analysis area of 300 μm × 700 μm and a pass energy 20 or 15 eV. CasaXPS (ver. 2.3.23) software was used for all deconvolution of spectra with N 1s linear background subtraction and all other high resolution with a Shirley background subtraction.

Thermogravimetric Analysis (TGA). Air-free TGA was performed on a TA Instruments Discovery TGA 55 instrument housed in a nitrogen-filled (99.998%) MBraun Labmaster 130 glovebox. In a typical experiment, approximately 25 mg of analyte was placed in a platinum pan and heated to 400 °C with a ramp rate of 10 °C/min. Nitrogen (99.999% purity, 60 sccm) was used as the process gas. Platinum pans were cleaned by sequential sonication in glacial acetic acid and then isopropanol, followed by heating until red-hot with a propane torch. Langmuir vapor pressure equations were derived from the TGA data using a previously reported method, employing benzoic acid as the calibrant.[5,6]

Differential Scanning Calorimetry (DSC). DSC experiments were performed with a TA Instruments Q10 instrument. The DSC was calibrated at the melting point of indium metal (156.6 °C). All DSC samples were hermetically sealed in aluminum pans inside a glovebox prior to analysis. All samples were heated to 500 °C with a ramp rate of 10 °C/min, using nitrogen (99.998% purity, 50 mL/min) as the process gas.

Time-of-Flight Secondary Ion Mass Spectrometry (ToF-SIMS). Samples were examined using an ION-TOF (GmbH) TOF-SIMS IV equipped with a Bi cluster liquid metal ion source. A pulsed 25 keV Bi_3^+ cluster primary ion beam was used to bombard the sample surface to generate secondary ions with a current of 1 μA. The positive (or negative) secondary ions were extracted from the sample surface, mass-separated, and detected via a reflectron-type time-of-flight analyzer. Reflector values for the positive and negative modes were +16 and −36 V, respectively. Sample charging was neutralized with a pulsed, low-energy electron flood. The ion mass spectra were collected in an area of 500 μm × 500 μm at 128 × 128 pixels with 20 scans. The high-resolution imaging spectra were collected with of 500 μm × 500 μm at 128 × 128 pixels with 100 scans, processed on the ION-TOF software and normalized to the total yield by a division normalization factor. The mass spectra were processed on ION-TOF software with a binning value of 256 and calibrated to H^+, C^+, and $C_2H_5^+$ mass signals.

Selectivity Measurements for ToF-SIMS Images. The assessment of NHC selectivity through ToF-SIMS imaging involved the categorization of metal bands as growth areas and dielectrics as nongrowth areas. Within the ION-TOF software, a region of interest (ROI) was designated for either metal or dielectric areas and subsequently correlated with the respective bands on the wafer. Ion intensities, specifically Ru^+ or Co^+ for metal bands and Si^+ or Al^+ for dielectric bands, were extracted from the ToF-SIMS mass spectra, with the metal and dielectric ROIs applied. To determine the selectivity values for the NHCs, the ROI of the metal bands ($\theta_{\text{Growth Area}}$) and the ROI of the dielectrics ($\theta_{\text{Non-Growth Area}}$) were applied to the patterned wafer. The ion intensity of the NHC was measured, and the signal was then normalized against the total ion yield, which encompasses metal (Co^+ or Ru^+), dielectric (Si^+ or Al^+), and NHC ions. The resulting selectivity value (S) should fall within the range of $1 \geq S \leq -1$, with 1 being perfect selectivity for the growth area and −1 being perfect selectivity for the nongrowth area. These values, representing both the ion yield fraction on the growth area and the nongrowth area, are utilized in eq 1.

Selectivity formula for the deposition of NHCs.

$$\text{selectivity} = \frac{\theta_{\text{growth area}} - \theta_{\text{non-growth area}}}{\theta_{\text{growth area}} + \theta_{\text{non-growth area}}} \qquad (1)$$

■ ASSOCIATED CONTENT

Supporting Information

The Supporting Information is available free of charge at https://pubs.acs.org/doi/10.1021/acs.chemmater.4c00412.

Details related to ToF-SIMS mass spectra, XPS, TGA, DSC data, QCM experiments, and AFM images (PDF)

■ AUTHOR INFORMATION

Corresponding Authors

Seán T. Barry – *Department of Chemistry, Carleton University, Ottawa, ON K1S 5B6, Canada; Carbon to Metal Coating Institute (C2MCI), Queen's University, Kingston, Ontario K7L 4 V1, Canada;* orcid.org/0000-0001-5515-4734; Email: sean_barry@carleton.ca

Cathleen M. Crudden – *Department of Chemistry, Queen's University, Kingston, ON K7L 3N6, Canada; Carbon to Metal Coating Institute (C2MCI), Queen's University, Kingston, Ontario K7L 4 V1, Canada;* orcid.org/0000-0003-2154-8107; Email: cruddenc@chem.queensu.ca

Paul J. Ragogna – *Department of Chemistry, University of Western Ontario, London, ON N6A 3K7, Canada; Carbon to Metal Coating Institute (C2MCI), Queen's University, Kingston, Ontario K7L 4 V1, Canada; Surface Science Western, London, ON N6G 0J3, Canada;* orcid.org/0000-0003-2727-7635; Email: pragogna@uwo.ca

Authors

Justin T. Lomax – *Department of Chemistry, University of Western Ontario, London, ON N6A 3K7, Canada; Carbon to Metal Coating Institute (C2MCI), Queen's University, Kingston, Ontario K7L 4 V1, Canada*

Eden Goodwin – *Department of Chemistry, Carleton University, Ottawa, ON K1S 5B6, Canada; Carbon to Metal Coating Institute (C2MCI), Queen's University, Kingston, Ontario K7L 4 V1, Canada*

Mark D. Aloisio – *Department of Chemistry, Queen's University, Kingston, ON K7L 3N6, Canada; Carbon to Metal Coating Institute (C2MCI), Queen's University, Kingston, Ontario K7L 4 V1, Canada*

Alex J. Veinot – *Department of Chemistry, Queen's University, Kingston, ON K7L 3N6, Canada; Carbon to Metal Coating Institute (C2MCI), Queen's University, Kingston, Ontario K7L 4 V1, Canada*

Ishwar Singh – *Department of Chemistry, Queen's University, Kingston, ON K7L 3N6, Canada; Carbon to Metal Coating Institute (C2MCI), Queen's University, Kingston, Ontario K7L 4 V1, Canada*

Wai-Tung Shiu – *Department of Chemistry, University of Western Ontario, London, ON N6A 3K7, Canada; Carbon to Metal Coating Institute (C2MCI), Queen's University, Kingston, Ontario K7L 4 V1, Canada*

Maram Bakiro – *Department of Chemistry, Carleton University, Ottawa, ON K1S 5B6, Canada; Carbon to Metal Coating Institute (C2MCI), Queen's University, Kingston, Ontario K7L 4 V1, Canada*

Jordan Bentley – *Department of Chemistry, Carleton University, Ottawa, ON K1S 5B6, Canada; Carbon to Metal Coating Institute (C2MCI), Queen's University, Kingston, Ontario K7L 4 V1, Canada*

Joseph F. DeJesus – *Department of Chemistry, Queen's University, Kingston, ON K7L 3N6, Canada*

Peter G. Gordon – *Department of Chemistry, Carleton University, Ottawa, ON K1S 5B6, Canada*

Lijia Liu – *Department of Chemistry, University of Western Ontario, London, ON N6A 3K7, Canada; Carbon to Metal Coating Institute (C2MCI), Queen's University, Kingston, Ontario K7L 4 V1, Canada; Surface Science Western, London, ON N6G 0J3, Canada;* orcid.org/0000-0003-2439-0739

Complete contact information is available at: https://pubs.acs.org/10.1021/acs.chemmater.4c00412

Author Contributions

The manuscript was written through contributions of all authors. All authors have given approval to the final version of the manuscript.

Notes

The authors declare no competing financial interest.

■ ACKNOWLEDGMENTS

The authors would like to thank the Semiconductor Research Corporation (SRC), the Natural Sciences and Engineering Council of Canada (NSERC), the New Frontiers in Research Fund-Transformation program (NFRFT-2020-00573), the Ontario Government Scholarship (OGS) program, the Canada Foundation for Innovation (CFI), Surface Science Western (SSW; Drs. M. Biesinger and J. Henderson), the Western Nanofabrication Facility, Carleton NanoFab, Western University, Queen's University, and Carleton University for their support.

REFERENCES

(1) Chakraborty, I.; Pradeep, T. Atomically Precise Clusters of Noble Metals: Emerging Link between Atoms and Nanoparticles. *Chem. Rev.* **2017**, *117* (12), 8208−8271.

(2) Yao, Q.; Chen, T.; Yuan, X.; Xie, J. Toward Total Synthesis of Thiolate-Protected Metal Nanoclusters. *Acc. Chem. Res.* **2018**, *51* (6), 1338−1348.

(3) Zhukhovitskiy, A. V.; MacLeod, M. J.; Johnson, J. A. Carbene Ligands in Surface Chemistry: From Stabilization of Discrete Elemental Allotropes to Modification of Nanoscale and Bulk Substrates. *Chem. Rev.* **2015**, *115* (20), 11503−11532.

(4) Häkkinen, H. The Gold−Sulfur Interface at the Nanoscale. *Nat. Chem.* **2012**, *4* (6), 443−455.

(5) Tolman, C. A. Steric Effects of Phosphorus Ligands in Organometallic Chemistry and Homogeneous Catalysis. *Chem. Rev.* **1977**, *77* (3), 313−348.

(6) van Leeuwen, P. W. Phosphines and Related Tervalent Phosphorus Systems. In *Organophosphorus Chemistry*; John Wiley & Sons, Ltd, 2019; pp 1−58.

(7) Crudden, C. M.; Allen, D. P. Stability and Reactivity of N-Heterocyclic Carbene Complexes. *Coord. Chem. Rev.* **2004**, *248* (21), 2247−2273.

(8) Hopkinson, M. N.; Richter, C.; Schedler, M.; Glorius, F. An Overview of N-Heterocyclic Carbenes. *Nature* **2014**, *510* (7506), 485−496.

(9) Jin, R.; Zeng, C.; Zhou, M.; Chen, Y. Atomically Precise Colloidal Metal Nanoclusters and Nanoparticles: Fundamentals and Opportunities. *Chem. Rev.* **2016**, *116* (18), 10346−10413.

(10) Nuzzo, R. G.; Allara, D. L. Adsorption of Bifunctional Organic Disulfides on Gold Surfaces. *J. Am. Chem. Soc.* **1983**, *105* (13), 4481−4483.

(11) Vignolle, J.; Tilley, T. D. N-Heterocyclic Carbene-Stabilized Gold Nanoparticles and Their Assembly into 3D Superlattices. *Chem. Commun.* **2009**, No. 46, 7230−7232.

(12) Crudden, C. M.; Horton, J. H.; Ebralidze, I. I.; Zenkina, O. V.; McLean, A. B.; Drevniok, B.; She, Z.; Kraatz, H.-B.; Mosey, N. J.; Seki, T.; Keske, E. C.; Leake, J. D.; Rousina-Webb, A.; Wu, G. Ultra Stable Self-Assembled Monolayers of N-Heterocyclic Carbenes on Gold. *Nat. Chem.* **2014**, *6* (5), 409−414.

(13) Inayeh, A.; Groome, R. R. K.; Singh, I.; Veinot, A. J.; de Lima, F. C.; Miwa, R. H.; Crudden, C. M.; McLean, A. B. Self-Assembly of N-Heterocyclic Carbenes on Au(111). *Nat. Commun.* **2021**, *12* (1), No. 4034.

(14) Larrea, C. R.; Baddeley, C. J.; Narouz, M. R.; Mosey, N. J.; Horton, J. H.; Crudden, C. M. N-Heterocyclic Carbene Self-Assembled Monolayers on Copper and Gold: Dramatic Effect of Wingtip Groups on Binding, Orientation and Assembly. *ChemPhysChem* **2017**, *18* (24), 3536−3539.

(15) Narouz, M. R.; Li, C.-H.; Nazemi, A.; Crudden, C. M. Amphiphilic N-Heterocyclic Carbene-Stabilized Gold Nanoparticles and Their Self-Assembly in Polar Solvents. *Langmuir* **2017**, *33* (50), 14211−14219.

(16) Zeng, Y.; Zhang, T.; Narouz, M. R.; Crudden, C. M.; McBreen, P. H. Generation and Conversion of an N-Heterocyclic Carbene on Pt(111). *Chem. Commun.* **2018**, *54* (88), 12527−12530.

(17) Trujillo, M. J.; Strausser, S. L.; Becca, J. C.; DeJesus, J. F.; Jensen, L.; Jenkins, D. M.; Camden, J. P. Using SERS To Understand the Binding of N-Heterocyclic Carbenes to Gold Surfaces. *J. Phys. Chem. Lett.* **2018**, *9* (23), 6779−6785.

(18) Bakker, A.; Timmer, A.; Kolodzeiski, E.; Freitag, M.; Gao, H. Y.; Mönig, H.; Amirjalayer, S.; Glorius, F.; Fuchs, H. Elucidating the Binding Modes of N-Heterocyclic Carbenes on a Gold Surface. *J. Am. Chem. Soc.* **2018**, *140* (38), 11889−11892.

(19) Amit, E.; Dery, L.; Dery, S.; Kim, S.; Roy, A.; Hu, Q.; Gutkin, V.; Eisenberg, H.; Stein, T.; Mandler, D.; Dean Toste, F.; Gross, E. Electrochemical Deposition of N-Heterocyclic Carbene Monolayers on Metal Surfaces. *Nat. Commun.* **2020**, *11* (1), No. 5714.

(20) Kang, H.; Jang, J.; Kong, G. D.; Jung, S.; Ohto, T.; Yoon, H. J. Deposition Condition Impacts Charge Tunneling and Thermoelectric Properties of N-Heterocyclic Carbene Monolayers. *J. Mater. Chem. A* **2023**, *11* (30), 16233−16242.

(21) Park, S.; Kang, S.; Yoon, H. J. Thermopower of Molecular Junction in Harsh Thermal Environments. *Nano Lett.* **2022**, *22* (10), 3953−3960.

(22) Kang, S.; Byeon, S. E.; Yoon, H. J. N-Heterocyclic Carbene Anchors in Electronics Applications. *Bull. Korean Chem. Soc.* **2021**, *42* (5), 712−723.

(23) MacLeod, M. J.; Goodman, A. J.; Ye, H.-Z.; Nguyen, H. V.-T.; Van Voorhis, T.; Johnson, J. A. Robust Gold Nanorods Stabilized by Bidentate N-Heterocyclic-Carbene−Thiolate Ligands. *Nat. Chem.* **2019**, *11* (1), 57−63.

(24) Smith, C. A.; Narouz, M. R.; Lummis, P. A.; Singh, I.; Nazemi, A.; Li, C.-H.; Crudden, C. M. N-Heterocyclic Carbenes in Materials Chemistry. *Chem. Rev.* **2019**, *119* (8), 4986−5056.

(25) Dery, S.; Kim, S.; Tomaschun, G.; Berg, I.; Feferman, D.; Cossaro, A.; Verdini, A.; Floreano, L.; Klüner, T.; Toste, F. D.; Gross, E. Elucidating the Influence of Anchoring Geometry on the Reactivity of NO2-Functionalized N-Heterocyclic Carbene Monolayers. *J. Phys. Chem. Lett.* **2019**, *10* (17), 5099−5104.

(26) Kaur, G.; L Thimes, R.; P Camden, J.; M Jenkins, D. Fundamentals and Applications of N-Heterocyclic Carbene Functionalized Gold Surfaces and Nanoparticles. *Chem. Commun.* **2022**, *58* (95), 13188−13197.

(27) Jiang, L.; Zhang, B.; Médard, G.; Seitsonen, A. P.; Haag, F.; Allegretti, F.; Reichert, J.; Kuster, B.; Barth, J. V.; Papageorgiou, A. C. N. -Heterocyclic Carbenes on Close-Packed Coinage Metal Surfaces: Bis-Carbene Metal Adatom Bonding Scheme of Monolayer Films on Au, Ag and Cu. *Chem. Sci.* **2017**, *8* (12), 8301−8308.

(28) Lara, P.; Rivada-Wheelaghan, O.; Conejero, S.; Poteau, R.; Philippot, K.; Chaudret, B. Ruthenium Nanoparticles Stabilized by N-Heterocyclic Carbenes: Ligand Location and Influence on Reactivity. *Angew. Chem., Int. Ed.* **2011**, *50* (50), 12080−12084.

(29) Asensio, J. M.; Tricard, S.; Coppel, Y.; Andrés, R.; Chaudret, B.; de Jesús, E. Synthesis of Water-Soluble Palladium Nanoparticles Stabilized by Sulfonated N-Heterocyclic Carbenes. *Chem. - Eur. J.* **2017**, *23* (54), 13435−13444.

(30) Martínez-Prieto, L. M.; Ferry, A.; Lara, P.; Richter, C.; Philippot, K.; Glorius, F.; Chaudret, B. New Route to Stabilize Ruthenium Nanoparticles with Non-Isolable Chiral N-Heterocyclic Carbenes. *Chem. - Eur. J.* **2015**, *21* (48), 17495−17502.

(31) Moock, D.; Wiesenfeldt, M. P.; Freitag, M.; Muratsugu, S.; Ikemoto, S.; Knitsch, R.; Schneidewind, J.; Baumann, W.; Schäfer, A. H.; Timmer, A.; Tada, M.; Hansen, M. R.; Glorius, F. Mechanistic Understanding of the Heterogeneous, Rhodium-Cyclic (Alkyl)(Amino)Carbene-Catalyzed (Fluoro-)Arene Hydrogenation. *ACS Catal.* **2020**, *10* (11), 6309−6317.

(32) Ernst, J. B.; Schwermann, C.; Yokota, G.; Tada, M.; Muratsugu, S.; Doltsinis, N. L.; Glorius, F. Molecular Adsorbates Switch on Heterogeneous Catalysis: Induction of Reactivity by N-Heterocyclic Carbenes. *J. Am. Chem. Soc.* **2017**, *139* (27), 9144−9147.

(33) Bernasconi, R.; Magagnin, L. Review—Ruthenium as Diffusion Barrier Layer in Electronic Interconnects: Current Literature with a Focus on Electrochemical Deposition Methods. *J. Electrochem. Soc.* **2019**, *166* (1), D3219.

(34) Auth, C.; Aliyarukunju, A.; Asoro, M.; Bergstrom, D.; Bhagwat, V.; Birdsall, J.; Bisnik, N.; Buehler, M.; Chikarmane, V.; Ding, G.; Fu, Q.; Gomez, H.; Han, W.; Hanken, D.; Haran, M.; Hattendorf, M.; Heussner, R.; Hiramatsu, H.; Ho, B.; Jaloviar, S.; Jin, I.; Joshi, S.; Kirby, S.; Kosaraju, S.; Kothari, H.; Leatherman, G.; Lee, K.; Leib, J.; Madhavan, A.; Marla, K.; Meyer, H.; Mule, T.; Parker, C.; Parthasarathy, S.; Pelto, C.; Pipes, L.; Post, I.; Prince, M.; Rahman, A.; Rajamani, S.; Saha, A.; Santos, J. D.; Sharma, M.; Sharma, V.; Shin, J.; Sinha, P.; Smith, P.; Sprinkle, M.; Amour, A. St.; Staus, C.; Suri, R.; Towner, D.; Tripathi, A.; Tura, A.; Ward, C.; Yeoh, A. In *A 10 nm High Performance and Low-Power CMOS Technology Featuring 3rd Generation FinFET Transistors, Self-Aligned Quad Patterning, Contact over Active Gate and Cobalt Local Interconnects*, 2017 IEEE International Electron Devices Meeting (IEDM); IEEE, 2017.

(35) Hu, C.-K.; Gignac, L.; Rosenberg, R. Electromigration of Cu/Low Dielectric Constant Interconnects. *Microelectron. Reliab.* **2006**, *46* (2), 213−231.

(36) Hu, C.-K.; Kelly, J.; Chen, J. H.-C.; Huang, H.; Ostrovski, Y.; Patlolla, R.; Peethala, B.; Adusumilli, P.; Spooner, T.; Gignac, L. M.; Bruley, J.; Breslin, C.; Cohen, S. A.; Lian, G.; Ali, M.; Long, R.; Hornicek, G.; Kane, T.; Kamineni, V.; Zhang, X.; Mont, F.; Siddiqui, S. In *Electromigration and Resistivity in On-Chip Cu, Co and Ru Damascene Nanowires*, 2017 IEEE International Interconnect Technology Conference (IITC); IEEE, 2017; pp 1−3.

(37) Moon, J. H.; Kim, S.; Kim, T.; Jeon, Y. S.; Kim, Y.; Ahn, J.-P.; Kim, Y. K. Electrical Resistivity Evolution in Electrodeposited Ru and Ru-Co Nanowires. *J. Mater. Sci. Technol.* **2022**, *105*, 17−25.

(38) van der Veen, M. H.; Heyler, N.; Pedreira, O. V.; Ciofi, I.; Decoster, S.; Gonzalez, V. V.; Jourdan, N.; Struyf, H.; Croes, K.; Wilson, C. J.; Tőkei, Z. In *Damascene Benchmark of Ru, Co and Cu in Scaled Dimensions*, 2018 IEEE International Interconnect Technology Conference (IITC); IEEE, 2018; pp 172−174.

(39) Ciofi, I.; Roussel, P. J.; Baert, R.; Contino, A.; Gupta, A.; Croes, K.; Wilson, C. J.; Mocuta, D.; Tőkei, Z. RC Benefits of Advanced Metallization Options. *IEEE Trans. Electron Devices* **2019**, *66* (5), 2339−2345.

(40) Hau-Riege, C. S. An Introduction to Cu Electromigration. *Microelectron. Reliab.* **2004**, *44* (2), 195−205.

(41) Cheng, Y.-L.; Huang, H.-C.; Lee, C.-Y.; Chen, G.-S.; Fang, J.-S. Comparison of Cu and Co Integration with Porous Low-k SiOCH Dielectrics. *Thin Solid Films* **2020**, *704*, No. 138010.

(42) Hu, C.-K.; Gignac, L.; Lian, G.; Cabral, C.; Motoyama, K.; Shobha, H.; Demarest, J.; Ostrovski, Y.; Breslin, C. M.; Ali, M.; Benedict, J.; McLaughlin, P. S.; Ni, J.; Liu, X. H. In *Mechanisms of Electromigration Damage in Cu Interconnects*, 2018 IEEE International Electron Devices Meeting (IEDM); IEEE, 2018.

(43) Liu, Y.-W.; Zhang, D.-J.; Tsai, P.-C.; Chiang, C.-T.; Tu, W.-C.; Lin, S.-Y. Nanometer-Thick Copper Films with Low Resistivity Grown on 2D Material Surfaces. *Sci. Rep.* **2022**, *12* (1), No. 1823.

(44) Parsons, G. N.; Clark, R. D. Area-Selective Deposition: Fundamentals, Applications, and Future Outlook. *Chem. Mater.* **2020**, *32*, 4920.

(45) Kedzierski, J.; Ieong, M.; Nowak, E.; Kanarsky, T. S.; Zhang, Y.; Roy, R.; Boyd, D.; Fried, D.; Wong, H.-S. P. Extension and Source/Drain Design for High-Performance FinFET Devices. *IEEE Trans. Electron Devices* **2003**, *50* (4), 952−958.

(46) Taiwan Semiconductor Manufacturing Company Limited. 3 nm Technology, 2023. http://www.tsmc.com/english/dedicatedFoundry/technology/logic/l_3nm.

(47) Murdoch, G.; Bömmels, J.; Wilson, C. J.; Gavan, K. B.; Le, Q. T.; Tőkei, Z.; Clark, W. In *Feasibility Study of Fully Self Aligned Vias for 5 nm Node BEOL*, 2017 IEEE International Interconnect Technology Conference (IITC); IEEE, 2017.

(48) Bui, H. V.; Grillo, F.; Ommen, J. R. van. Atomic and Molecular Layer Deposition: Off the Beaten Track. *Chem. Commun.* **2016**, *53* (1), 45−71.

(49) Liu, T.-L.; Bent, S. F. Area-Selective Atomic Layer Deposition on Chemically Similar Materials: Achieving Selectivity on Oxide/Oxide Patterns. *Chem. Mater.* **2021**, *33*, 513.

(50) Yan, M.; Koide, Y.; Babcock, J. R.; Markworth, P. R.; Belot, J. A.; Marks, T. J.; Chang, R. P. H. Selective-Area Atomic Layer Epitaxy Growth of ZnO Features on Soft Lithography-Patterned Substrates. *Appl. Phys. Lett.* **2001**, *79* (11), 1709−1711.

(51) Minaye Hashemi, F. S.; Birchansky, B. R.; Bent, S. F. Selective Deposition of Dielectrics: Limits and Advantages of Alkanethiol Blocking Agents on Metal−Dielectric Patterns. *ACS Appl. Mater. Interfaces* **2016**, *8* (48), 33264−33272.

(52) Lecordier, L.; Herregods, S.; Armini, S. Vapor-Deposited Octadecanethiol Masking Layer on Copper to Enable Area Selective Hf3N4 Atomic Layer Deposition on Dielectrics Studied by in Situ Spectroscopic Ellipsometry. *J. Vac. Sci. Technol., A* **2018**, *36* (3), No. 031605.

(53) Chen, R.; Bent, S. F. Chemistry for Positive Pattern Transfer Using Area-Selective Atomic Layer Deposition. *Adv. Mater.* **2006**, *18* (8), 1086−1090.

(54) Seo, E. K.; Lee, J. W.; Sung-Suh, H. M.; Sung, M. M. Atomic Layer Deposition of Titanium Oxide on Self-Assembled-Monolayer-Coated Gold. *Chem. Mater.* **2004**, *16* (10), 1878−1883.

(55) Lee, H.-B.-R.; Mullings, M. N.; Jiang, X.; Clemens, B. M.; Bent, S. F. Nucleation-Controlled Growth of Nanoparticles by Atomic Layer Deposition. *Chem. Mater.* **2012**, *24* (21), 4051−4059.

(56) Avila, J. R.; DeMarco, E. J.; Emery, J. D.; Farha, O. K.; Pellin, M. J.; Hupp, J. T.; Martinson, A. B. F. Real-Time Observation of Atomic Layer Deposition Inhibition: Metal Oxide Growth on Self-Assembled Alkanethiols. *ACS Appl. Mater. Interfaces* **2014**, *6* (15), 11891−11898.

(57) Noh, J.; Kato, H. S.; Kawai, M.; Hara, M. Surface Structure and Interface Dynamics of Alkanethiol Self-Assembled Monolayers on Au(111). *J. Phys. Chem. B* **2006**, *110* (6), 2793−2797.

(58) Prathima, N.; Harini, M.; Rai, N.; Chandrashekara, R. H.; Ayappa, K. G.; Sampath, S.; Biswas, S. K. Thermal Study of Accumulation of Conformational Disorders in the Self-Assembled Monolayers of C8 and C18 Alkanethiols on the Au(111) Surface. *Langmuir* **2005**, *21* (6), 2364−2374.

(59) Lovat, G.; Doud, A.; Lu, E.; Kladnik, D.; Inkpen, M. S.; et al. Determination of the Structure and Geometry of N-Heterocyclic Carbenes on Au(111) Using High-Resolution Spectroscopy. *Chem. Sci.* **2019**, *10* (3), 930−935.

(60) Berg, I.; Amit, E.; Hale, L.; Toste, F. D.; Gross, E. N-Heterocyclic Carbene Based Nanolayer for Copper Film Oxidation Mitigation. *Angew. Chem., Int. Ed.* **2022**, *61* (25), No. e202201093.

(61) Nguyen, D. T.; Freitag, M.; Körsgen, M.; Lamping, S.; Rühling, A.; Schäfer, A. H.; Siekman, M. H.; Arlinghaus, H. F.; van der Wiel, W. G.; Glorius, F.; Ravoo, B. J. Versatile Micropatterns of N-Heterocyclic Carbenes on Gold Surfaces: Increased Thermal and Pattern Stability with Enhanced Conductivity. *Angew. Chem., Int. Ed.* **2018**, *57* (35), 11465−11469.

(62) Crudden, C. M.; Horton, J. H.; Narouz, M. R.; Li, Z.; Smith, C. A.; Munro, K.; Baddeley, C. J.; Larrea, C. R.; Drevniok, B.; Thanabalasingam, B.; McLean, A. B.; Zenkina, O. V.; Ebralidze, I. I.; She, Z.; Kraatz, H.-B.; Mosey, N. J.; Saunders, L. N.; Yagi, A. Simple Direct Formation of Self-Assembled N-Heterocyclic Carbene Monolayers on Gold and Their Application in Biosensing. *Nat. Commun.* **2016**, *7* (1), No. 12654.

(63) Fèvre, M.; Pinaud, J.; Leteneur, A.; Gnanou, Y.; Vignolle, J.; Taton, D.; Miqueu, K.; Sotiropoulos, J.-M. Imidazol(in)Ium Hydrogen Carbonates as a Genuine Source of N-Heterocyclic Carbenes (NHCs): Applications to the Facile Preparation of NHC Metal Complexes and to NHC-Organocatalyzed Molecular and Macromolecular Syntheses. *J. Am. Chem. Soc.* **2012**, *134* (15), 6776−6784.

(64) Price, D. M. Vapor Pressure Determination by Thermogravimetry. *Thermochim. Acta* **2001**, *367−368*, 253−262.

(65) Price, D. M. A Fit of the Vapours. *Thermochim. Acta* **2015**, *622*, 44−50.

(66) Weidner, T.; Baio, J. E.; Mundstock, A.; Große, C.; Karthäuser, S.; Bruhn, C.; Siemeling, U.; Weidner, T.; Baio, J. E.; Mundstock, A.; Große, C.; Karthäuser, S.; Bruhn, C.; Siemeling, U. NHC-Based Self-Assembled Monolayers on Solid Gold Substrates. *Aust. J. Chem.* **2011**, *64* (8), 1177−1179.

(67) Choi, Y.; Park, C. S.; Tran, H.-V.; Li, C.-H.; Crudden, C. M.; Lee, T. R. Functionalized N-Heterocyclic Carbene Monolayers on Gold for Surface-Initiated Polymerizations. *ACS Appl. Mater. Interfaces* **2022**, *14* (39), 44969−44980.

(68) Veinot, A. J.; Al-Rashed, A.; Padmos, J. D.; Singh, I.; Lee, D. S.; Narouz, M. R.; Lummis, P. A.; Baddeley, C. J.; Crudden, C. M.; Horton, J. H. N-Heterocyclic Carbenes Reduce and Functionalize Copper Oxide Surfaces in One Pot. *Chem. - Eur. J.* **2020**, *26* (50), 11431−11434.